2916 *Chem. Mater.* **2010,** *22,* 2916–2922
DOI:10.1021/cm100226h

CHEMISTRY OF MATERIALS
Article

Formation of Ultrathin Birnessite-Type Nanoparticles Immobilized on Spherical Polyelectrolyte Brushes†

Frank Polzer,‡ Daniel A. Kunz,§ Josef Breu,§ and Matthias Ballauff*,‡

‡*Helmholtz-Zentrum Berlin für Materialien und Energie GmbH, Hahn-Meitner-Platz 1, 14109 Berlin, Germany, and Department of Physics, Humboldt University Berlin, Newtonstr. 15, 12489 Berlin, Germany,* and §*Department of Inorganic Chemistry I, University of Bayreuth, 95440 Bayreuth, Germany*

Received January 25, 2010. Revised Manuscript Received March 9, 2010

A new route of in situ formation and stabilization of ultrathin, needle-like manganese dioxide nanoparticles (MnO_2NP) in aqueous solution by using spherical polyelectrolyte brush particles (SPB) is presented. The SPB that act as carrier particles consist of a solid polystyrene core of about 50 nm radius onto which long chains of the positively charged polyelectrolyte poly(trimethyl ammonium ethyl methacrylate chloride) (pTMAEMC) are grafted to yield an overall radius of about 85 nm. Potassium permanganate ($KMnO_4$) is directly reduced within the brush layer of these particles because of the basic environment within this layer. This mechanism appears to limit the size of the MnO_2NP to the dimensions of the brush layer. Powder X-ray diffraction, (PXRD), transmission electron microscopy (TEM), and cryogenic transmission electron microscopy (cryoTEM) prove that birnessite-type MnO_2NP with a c*-disorder are generated on the SPB without adding any reducing agent. The birnessite nanoparticles have an average length of 20 nm and a breadth of about 1.6 nm. They are composed of single lamellae or of ultrathin stacks of very few lamellae. Energy-dispersive X-ray spectroscopy (EDX) demonstrates that most of the charges of the thin birnessite platelets are balanced by potassium ions. The excellent stabilization by the SPB carrier particles in aqueous solution can be traced back to a strong interaction of the birnessite particles with the positively charged pTMAEMC chains of the SPB.

Introduction

Manganese oxide materials and especially manganese dioxide (MnO_2) that appears in a wide variety of polymorphs such as α-, β-, γ-, and δ-MnO_2 have attracted great interest recently. This is due to the possible applications as, for example, electrode materials,[1,2] catalysts,[3,4] ion exchange,[5] and magnetic materials.[6,7] All different polymorphs are based on the MnO_6 octahedron and differ in the linkage of these basic units.[8] In principle, the synthesis can be achieved by the oxidation of Mn^{2+}, by the reduction of permanganate (MnO_4^-), or by direct conversion of manganese oxides (Mn_2O_3, MnOOH, etc.).[9−11] The physical and chemical properties of these materials change when downsized to the nanoscopic scale, and great efforts have been made to design MnO_2 nanometer-sized structures of different size and shape.[12−16] Hence, a number of different morphologies have been realized, as, for example, one-dimensional (1D) structures (nanorods, nanowires, nanofibers, etc.), two-dimensional (2D) structures (nanosheets, etc.), and three-dimensional (3D) structures (ball-like core−corona particles, nanodisks, etc.).[8,17−20]

Among these manganese oxides, birnessite has attracted particular attention because of its unique properties and its use as an intermediate for the preparation of

† Dedicated to Professor Rüdiger Kniep on the occasion of his 65th birthday.

*To whom correspondence should be addressed. E-mail: matthias.ballauff@helmholtz-berlin.de.

(1) Débart, A.; Paterson, A. J.; Bao, J.; Bruce, P. G. *Angew. Chem.* **2008**, *120*, 1–5.
(2) Fischer, A. E.; Pettigrew, K. A.; Rolison, D. R.; Stroud, R. M.; Long, J. W. *Nano Lett.* **2007**, *7*, 281–286.
(3) Son, Y. C.; Makwana, V. D.; Howell, A. R.; Suib, S. L. *Angew. Chem.* **2001**, *40*, 4280–4283.
(4) Espinal, L.; Suib, S. L.; Rusling, J. F. *J. Am. Chem. Soc.* **2004**, *126*, 7676–7682.
(5) Shen, Y. F.; Zerger, R. P.; DeGuzman, R. N.; Suib, S. L.; McCurdy, L.; Potter, D. I.; O'Young, C. L. *Science* **1993**, *260*, 511–515.
(6) Zhu, H. T.; Luo, J.; Yang, H. X.; Laing, J. K.; Rao, G. H.; Li, J. B.; Du, Z. M. *J. Phys. Chem. C* **2008**, *112*, 17089–17094.
(7) Ge., J.; Zhou, L.; Yang, F.; Tang, B.; Wu, L.; Tung, C. *J. Phys. Chem. B* **2006**, *110*, 17854–17859.
(8) Wang, N.; Cao, X.; He, L.; Zhang, W.; Gou, L.; Chen, C.; Wang, R.; Yang, S. *J. Phys. Chem. C* **2008**, *112*, 365–369.
(9) Liu, Z.-H.; Ooi, K.; Kanoh, H.; Tang, W.; Yang, X.; Tomida, T. *Chem. Mater.* **2001**, *13*, 473–478.
(10) Chen, R.; Zavalji, P.; Whittingham, M. S. *Chem. Mater.* **1996**, *8*, 1275–1280.
(11) Ma, R.; Bando, Y.; Zhang, L.; Sasaki, T. *Adv. Mater.* **2004**, *16*, 918–922.
(12) Burda, C.; Chen, X.; Narayanan, R; El-Sayed, M. A. *Chem. Rev.* **2005**, *105*, 1025–1102.
(13) Alivisatos, A. P. *Science* **1996**, *271*, 933–937.
(14) Liang, S.; Teng, F.; Bulgan, G.; Zong, R.; Zhu, Y. *J. Phys. Chem. C* **2008**, *112*, 5307–5315.
(15) Luo, J.; Zhu., H. T.; Fan, H. M.; Liang, J. K.; Shi, H. L.; Rao, G. H.; Li, J. B.; Du, Z. M.; Shen, Z. X. *J. Phys. Chem. C* **2008**, *112*, 12594–12598.
(16) Portevault, D.; Cassaignon, S.; Nassif, N.; Baudrin, E.; Jolivet, J.-P. *Angew. Chem., Int. Ed.* **2008**, *47*, 6441–6444.
(17) Wang, X.; Li, Y. *J. Am. Chem. Soc.* **2002**, *124*, 2880–2881.
(18) Oaki, Y.; Imai, H. *Angew. Chem., Int. Ed.* **2007**, *46*, 4951–4955.
(19) Fukuda, K.; Nakai, I.; Ebina, Y.; Tananka, M.; Mori, T.; Sasaki, T. *J. Phys. Chem. B* **2006**, *110*, 17070–17075.
(20) Portevault, D.; Cassaignon, S.; Baudrin, E.; Jolivet, J.-P. *Chem. Mater.* **2008**, *20*, 6140–6147.

Published on Web 03/25/2010

other MnO_2 based materials such as octahedral molecular sieves.[21,22] Birnessite is a phyllomanganate meaning a layered structure of hydrous manganese oxide composed of edge-sharing octahedra containing predominantly Mn^{4+} cations as central ions. Because of the presence of Mn^{3+} cations and/or vacant octahedral sites a net layer charge arises that is compensated by the incorporation of different cations into the interlamellar space. Typically, these interlayer cations are hydrated.[23−26] The interlayer cations can be exchanged against various other ions such as tetraalkylammonium ions (TAA) or positively charged aluminum based oligo-cations such as Keggin ions.[27−30] The intercalation of bulky counterions can furthermore be used to expand the interlayer space and finally delaminate the hexagonal sheets to gain single lamellae of birnessite.[31] This delamination process is well-known from layered silicates or similarly structured materials, for example, layered double hydroxides (LDHs). Moreover, it is important for the generation of ultrathin films and for the building of layer-by-layer structures.[32] The generation of delaminated or exfoliated (stacks of only a few lamellae) birnessites is usually a tedious multistep process which involves the intercalation of bulky ions and subsequent delamination.[28,33,34] To our best knowledge there is only one report in the literature of single step routes to created ultrathin birnessite materials.[35] Aqueous suspensions of these particles do not exhibit a high colloidal stability and are difficult to handle because of their high surface area and the large lateral dimensions of the platelets of up to 0.5 μm. Applications in, for example, catalysis, however, require stable colloidal systems that can be easily synthesized at a kilogram scale.

In this paper we present the synthesis and comprehensive characterization of ultrathin birnessite nanoneedles that are affixed to spherical polyelectrolyte brushes (SPB).[36] The SPBs used herein consist of a solid polystyrene core (PS core) onto which long polyelectrolyte chains (PE chains) are densely grafted (Figure 1). Here we use the strong polyelectrolyte poly(2-trimethylammonium ethyl methacrylate chloride) (pTMAEMC) which carries positive charges. Recent work has shown that the immobilization of metallic or oxidic nanoparticles on SPB is a promising way towards colloidally stable composite particles with a high catalytic activity.[37−41] Moreover, cationic polyelectrolytes have recently been used successfully to create and stabilize thin films of birnessite.[42,43] Here we demonstrate that cationic spherical polyelectrolyte brushes can be used to prepare and immobilize ultrathin birnessite needles by adding $KMnO_4$ solution to the aqueous suspension of the SPB. The resulting composite particles exhibit an excellent colloidal stability and open new venues for the use of birnessite as catalyst in aqueous systems.

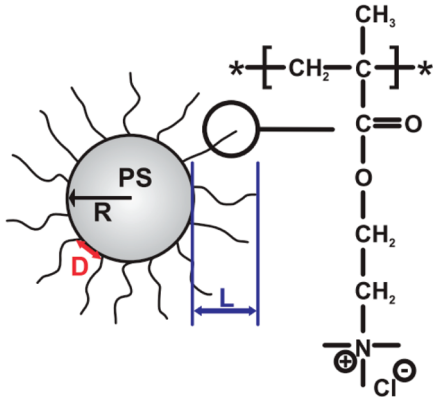

Figure 1. Scheme of a cationic spherical polyelectrolyte brush with brush monomer 2-trimethylammonium ethyl methacrylate chloride (TMAEMC). Here *R* represents the hydrodynamic radius of the polystyrene core, *L* stands for the contour length of the polyelectrolyte chains, and *D* is the average distance of junctions of polyelectrolyte chains on the surface of the core particle.

Experimental Section

Materials. All chemicals were of analytical grade and used without further purification. 2-Trimethylammonium ethyl methacrylate chloride (TMAEMC) was received from Polysciences. $KMnO_4$ was purchased from Fluka and used as received. Water used in all of our work described here was 18 MΩ Millipore water.

Synthesis of the Cationic SPB. Cationic SPB TMAEMC-40 was synthesized and characterized as described recently.[44] In a typical run, 62.5 g of 2-[*p*-(2-Hydroxy-2-methylpropiophenone)]-Ethylene Glycol-Methacrylate (HMEM) functionalized polystyrene latex were dispersed in water to give a solid content of 3.5 wt %. After addition of 56.0 g of TMAEMC to the

(21) Cai, J.; Liu, J.; Suib, S. L. *Chem. Mater.* **2002**, *14*, 2071–2077.
(22) Yang, D. S.; Wang, M. K. *Chem. Mater.* **2001**, *13*, 2589–2594.
(23) Post, J. E.; Veblen, D. R. *Am. Mineral.* **1990**, *75*, 477–489.
(24) Ching, S.; Petrovay, D. J.; Jorgensen, M. L.; Suib, S.-L. *Inorg. Chem.* **1997**, *36*, 883–890.
(25) Gaillot, A.-C.; Drits, V. A.; Plancon, A.; Lanson, B. *Chem. Mater.* **2004**, *16*, 1890–1905.
(26) Gaillot, A.-C.; Flot, D.; Drits, V. A.; Manceau, A.; Burghammer, M.; Lanson, B. *Chem. Mater.* **2003**, *15*, 4666–4678.
(27) Tang, W. P.; Kanoh, H.; Yang, X. J.; Ooi, K. *Chem. Mater.* **2000**, *12*, 3271–3279.
(28) Liu, Z. H.; Ooi, K.; Kanoh, H.; Tang, W.-P.; Tomida, T. *Langmuir* **2000**, *16*, 4154–4164.
(29) Brock, S. L.; Sanabria, M.; Urban, V.; Thiyagarajan, P.; Potter, D. I.; Suib, S. L. *Phys. Chem. B* **1999**, *103*, 7416–7428.
(30) Wong, S. T.; Cheng, S. *Inorg. Chem.* **1992**, *31*, 1164–1172.
(31) Liu, Z.; Ma, R.; Ebina, Y.; Takada, K.; Sasaki, T. *Chem. Mater.* **2007**, *19*, 6504–6512.
(32) Möller, M. W.; Handge, U. A.; Kunz, D. A.; Lunkenbein, T.; Altstädt, V.; Breu, J. *ASC Nano* **2010**, *4*, 717–724.
(33) Gao, Q.; Giraldo, O.; Tong, W.; Suib, S. L. *Chem. Mater.* **2001**, *13*, 778–786.
(34) Omomo, Y.; Sasaki, T.; Wang, L. Z.; Watanabe, M. *J. Am. Chem. Soc.* **2003**, *125*, 3568–3575.
(35) Kai, K.; Yoshida, Y.; Kageyama, H.; Saito, G.; Ishigaki, T.; Furukawa, Y.; Kawamata, J. *J. Am. Chem. Soc.* **2008**, *130*, 15938–15943.
(36) Ballauff, M. *Prog. Polym. Sci.* **2007**, *32*, 1135–1151.
(37) Lu, Y.; Wittemann, A.; Ballauff, M. *Macromol. Rapid Commun.* **2009**, *30*, 806–815.
(38) Schrinner, M.; Polzer, F.; Mei, Y.; Lu, Y.; Haupt, B.; Göldel, A.; Drechsler, M.; Preussner, J.; Glatzel, U.; Ballauff, M. *Macromol. Chem. Phys.* **2007**, *208*, 1542–1547.
(39) Schrinner, M.; Proch, S.; Mei, Y.; Kempe, R.; Miyajima, N.; Ballauff, M. *Adv. Mater.* **2008**, *20*, 1928–1933.
(40) Mei, Y.; Sharma, G.; Lu, Y.; Drechsler, M.; Irrgang, T.; Kempe, R.; Ballauff, M. *Langmuir* **2005**, *21*, 12229–12234.
(41) Schrinner, M.; Möller, M.; Thun, J.; Kauffmann, Y.; Breu, J.; Talmon, Y.; Ballauff, M. *Science* **2009**, *323*, 617–620.
(42) Nakayama, M.; Tagashira, H. *Langmuir* **2006**, *22*, 3864–3869.
(43) Lvov, Y.; Munge, B.; Giraldo, O.; Ichinose, I.; Suib, S. L.; Rusling, J. F. *Langmuir* **2000**, *16*, 8850–8857.
(44) Sharma, G.; Ballauff, M. *Macromol. Rapid Commun.* **2004**, *25*, 547–557.

dispersion, the mixture was degassed and cooled down to 8 °C. The polymerization was started by irradiation of the dispersion by UV light.[45] The reaction was irradiated and cooled for 30 min. The dispersion was purified by ultrafiltration (UF) until the conductivity of the serum reached values lower than 3 μS cm^{-1}.

Synthesis of the MnO_2NP Immobilized on SPB. The dispersion of SPB was diluted with water to a solid content of about 1.0 wt %. The mixture was bubbled with nitrogen under stirring for half an hour to remove oxygen. Afterward, 20 mL of a 0.04 M solution of $KMnO_4$ were injected, and the solution was stirred for 12 h. The composite particles were cleaned with water by UF until the conductivity of the serum reached a value of lower than 3 μS cm^{-1}.

Synthesis of the H^+-Birnessite. This compound was synthesized according to McKenzie et al.[46] In a typical reaction, 1.58 g of $KMnO_4$ were dissolved in 100 mL of water, and 1.64 mL of concentrated hydrochloric acid (HCl) were added dropwise to the solution. The precipitate was filtered and cleaned by dialysis against water.

Synthesis of the K^+-Birnessite. K^+-birnessite was synthesized by the thermal decomposition of $KMnO_4$ at 800 °C for 16 h. In a typical run, 5.0 g of $KMnO_4$ were heated at 2 °Cmin^{-1} to 800 °C and kept for 16 h at this temperature, before cooling down with 1 °Cmin^{-1}. The product was washed with water until the filtrate became clear.[47]

Methods. Transmission electron microscopy (TEM) and cryogenic transmission electron microscopy (cryoTEM) measurements were conducted with a Zeiss EM922 EFTEM (Zeiss NTS GmbH, Oberkochen, Germany) as described recently.[48] Dynamic light scattering (DLS) was performed with an ALV 4000 (Peters) light scattering goniometer. Samples for Powder X-ray diffraction PXRD were prepared onto a silicon zero-background plate via a back-loading technique to minimize textural effects. PXRD patterns were obtained using nickel filtered Cu$-K_\alpha$ radiation (1.54187 Å) on a Bragg$-$Brentano-type diffractometer (Panalytical XPERT-PRO) equipped with an X'Celerator Scientific RTMS detector. Energy Dispersive X-ray spectroscopy (EDX) was conducted with a Zeiss 1530 FESEM. The number of amino groups of the SPB, and therefore the core to shell ratio, was determined by potentiometric titration of TMAEMC-40 with 0.01 M silver nitrate ($AgNO_3$) standard solution (Merck) using a WTW cond 197i conductometer. The amount of MnO_2 immobilized on the SPB was determined by thermal gravimetric analysis (TGA) using a Mettler Toledo STARe system. Zeta potential measurements were performed with a Malvern Zetasizer Nano ZS.

Results and Discussion

Synthesis. The synthesis of the cationic spherical polyelectrolyte brushes was conducted as described in previous work.[44] The hydrodynamic radius R_h of the polystyrene-co-HMEM core due to DLS measurements is 42.7 nm ±0.3 nm. After the photoemulsion polymerization, R_h of the cationic SPB increased to 84.7 nm ±0.5 nm because of the grafting-to process of polyelectrolyte chains consisting of pTMAEMC onto the core particles. The pTMAEMC shell thus grafted to the surface of the core particles has a R_h of 42.0 nm ±0.8 nm. Potentiometric Titration with 0.01 M $AgNO_3$ standard solution gives the total number of charges on one particle. This analysis showed that the SPB used in this study had a core-to-shell mass weighted ratio of 6.6 to 1. Thus, the weight fraction of the shell is approximately one-third of the weight. The precise determination of this mass ratio is important for the mechanistic studies given below.

After adding the $KMnO_4$ solution to the dispersion of the cationic SPB (see Figure 2), the process of the reduction of the MnO_4^- ions could be directly seen by the fading of the color from purple to brown. The MnO_4^- ions are exchanged against the chloride counterions of the polyelectrolyte brush and a p(TMAEM MnO_4) precursor is formed with the quaternized ammonium groups of the polymer chains. We conclude that this reaction step is similar to the synthesis of layered MnO_2 structures using low molecular weight tetraalkylammonium halogenides according to Brock et al.[29] Thus, the precursor is reduced in situ inside the brush layer and MnO_2 nanoparticles are formed. This reaction seems to be promoted by the slight basic environment within the brush layer which results from possible diffusion of OH^- ions into the positively charged brush. Additionally, the generated MnO_2 nanoparticles may be able to act as a catalyst for further reduction of $KMnO_4$.

To elucidate this reaction further, we studied the influence of different reaction conditions for the formation of the MnO_2NP. We varied the amount of added $KMnO_4$ solution, the rate of addition, and the temperature. Increasing the amount of MnO_4^- ions leads to an increase of the total amount of MnO_2NP. An important finding is that the amount of inorganic nanoparticles still increases even if the molar amount of $KMnO_4$ exceeds the amount of functional groups in the brush layer. This is a clear indication that $KMnO_4$ does not react with the monomer units of the brush. Varying the amount of $KMnO_4$ does not have a significant influence on the size or the structure of the formed MnO_2NP, which was proven by cryoTEM and PXRD (see below). The overall size of the nanoparticles is only limited by the dimensions of the SPB, which again demonstrates that their formation proceeds along the polyelectrolyte chains via a p(TMAEM MnO_4) precursor. Moreover, the dosage time of the $KMnO_4$ solution did not affect any properties of the nanoparticles. Furthermore there were no noteworthy effects related to the dosage rate of the $KMnO_4$ solution. The generation of the particle seems to proceed very fast since a color shift is visible within a few seconds after the $KMnO_4$ addition. Increasing the temperature to 90 °C leads to a slight increase of the total amount of MnO_2NP formed on the SPB without changing the shape or the grade of crystallinity of the nanoparticles (see Supporting Information, Figure S2). Working at elevated temperatures, however, has negative influence on the stability of the composite system since coagulation processes are promoted.

The mechanism of particle formation thus implies that the reduction takes place only in the brush layer of the SPB,

(45) Schrinner, M.; Haupt, B.; Wittemann, A. *Chem. Eng. J.* **2008**, *144*, 138–145.
(46) McKenzie, R. M. *Mineral. Mag.* **1978**, *38*, 493–502.
(47) Kim, S. H.; Kim, S. J.; Oh, S. M. *Chem. Mater.* **1999**, *11*, 557–563.
(48) Wittemann, A.; Drechsler, M.; Talmon, Y.; Ballauff, M. *J. Am. Chem. Soc.* **2005**, *127*, 9688–9689.

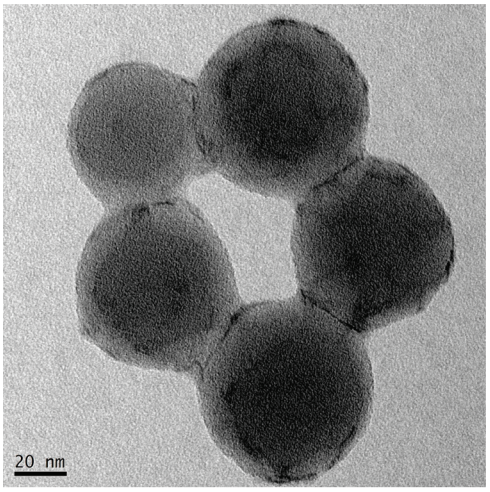

(a)

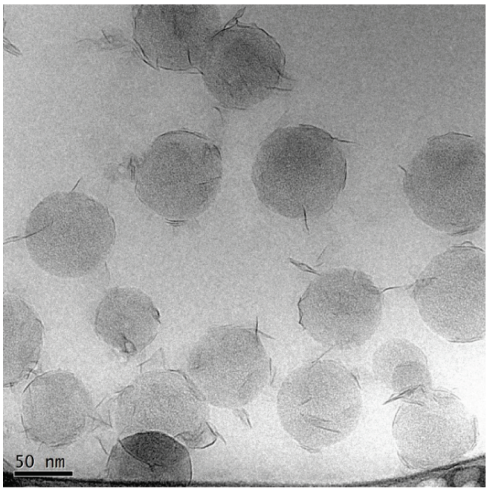

(b)

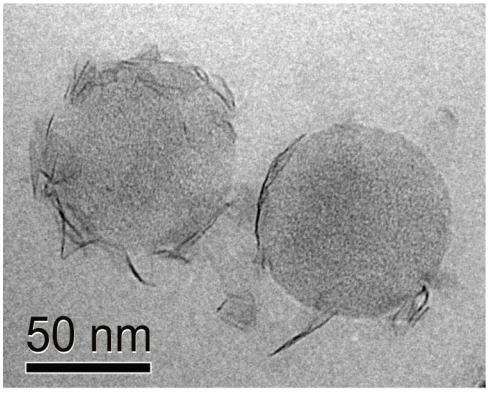

(c)

Figure 2. TEM of the composite system SPB-MnO_2-8 (a) and cryoTEM of the same system (b and c) shows the structural difference of the MnO_2NP immobilized on the SPB in the dried and the dispersed state. Whereas TEM indicates a more isotropic structure of the nanoparticles, the vitrified sample shows the formation of MnO_2 nanoneedles immobilized on the SPBs.

and the generated nanoparticles are directly stabilized by the pTMAEMC chains. This explains why there are virtually no free MnO_2NP in solution as will become evident by the analysis of the system by TEM and cryoTEM below. Another explanation for this finding is that MnO_2NP usually possess a negative surface charge.[29] Therefore these particles are bound to the SPB by ionic interaction of the oppositely charged pTMAEMC shell. Measurements of the zeta potential support this conclusion since there is a notable decrease of the potential after the MnO_2NP have been generated within the polyelectrolyte shell of the SPB. Moreover, DLS-measurements demonstrated that the hydrodynamic radius of the SPB decreases from 82.7 to 66.0 nm after the formation of the nanoparticles. This fact can be explained by the interaction of the positively charged pTMAEMC chains with the negatively charged MnO_2NP leading to a bridging of the chains of the shell and a decrease of the hydrodynamic radius as schematically depicted in Figure 4. Schrinner et al. discussed this effect in their studies of the mechanism of the formation of gold nanoparticles within cationic SPBs.[38] The strong interaction of the MnO_2NP with the polyelectrolyte chains leads to an excellent colloidal stability of the composite particles that allows us to purify them by extensive ultrafiltration against pure water. This point will become important when analyzing the structure of the MnO_2NP.

TEM and cryoTEM studies. We now turn to the analysis of the particles by transmission electron microscopy (TEM). Figure 2a displays the TEM pictures of the particles that refer to the dry state whereas cryoTEM images in Figure 2b and 2c display the structure of the composite particles in the aqueous phase, that is, directly in situ. The cryoTEM micrographs show that the MnO_2NP are of needle-like shape and have a typical breadth of 1.6 nm and an average length of 20 nm. The thickness of the particles derived from the cryoTEM micrographs indicates that the nanoparticles consist mainly of single lamellae or ultrahin stacks of very limited numbers of lamellae. We conclude from the habitus of the nanocrystals together with the analysis by wide-angle X-ray scattering (PXRD) given below that the modification of MnO_2 given here is birnessite. Since structures with a thickness of a few nm of birnessite show a poor electron contrast in cryoTEM, only particles vertically aligned with their *ab* plane to the electron beam are clearly visible. This becomes evident looking at Figure 2c. The dark, thin needle-like particles are stacks of octahedral layers of MnO_2 where the basal planes are within the angle of vision. In some cases individual birnessite particles are aligned parallel to each other. This indicates a layer-by-layer structure of the polyelectrolyte and the nanoparticles resulting from their opposite charge. This is in good agreement with the proposed particle generation mechanism which is shown in Supporting Information, Figure S1. In contrast to that, thin lamellae oriented horizontally with the *ab* plane to the electron beam are hardly visible (Figure 2c). This is also due to the high background caused by the solid polystyrene lattices. As already mentioned above, the length of the MnO_2NP does not exceed the dimensions of the brush layer which proves the mechanism of a polymer-assisted nanoparticle growth and stabilization. In addition, there are no free MnO_2NP in the solution, which is in good agreement with previous

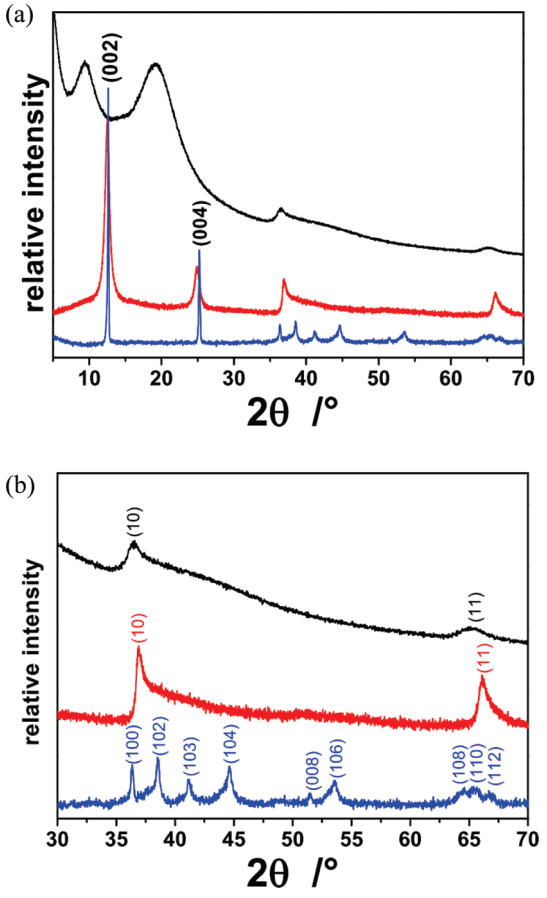

Figure 3. (a) PXRD patterns of the composite particle (black line), the c^*-disordered H^+-birnessite (red line) and the c^*-ordered K^+-birnessite (blue line). The two broad peaks of the composite material in the first part of the pattern can be assigned to the bare SPB, whereas the *hk*-bands at 36° and 65° 2θ are due to the c^*-disordered birnessite nanoneedles (b). Please note the lack of any *00l* reflections for the composite material.

results of other work.[40,42,49] This point is important for possible applications, because separation of the nanoparticles from the solution is simplified by immobilizing them on SPB by, for example, centrifugation.

The comparison between the TEM and the cryoTEM micrographs demonstrates that the structure obtained by both methods differs strongly. Obviously, the drying necessary for the TEM pictures leads to a collapse of the fine needle-like nanoparticles. Moreover, the drying leads to a loss of the interlayer water in the birnessite structures which will quickly evaporate under the conditions of TEM.

Structural Characterization by X-ray Diffraction. The assignment of the modification can be corroborated by wide-angle diffractograms to be discussed in the following. To elucidate the structure of the nanoparticles generated on the SPB, two well-known birnessite modifications (H^+-birnessite, see ref 46; K^+-birnessite, see ref 47) have been synthesized for comparison. The PXRD patterns of the composite particles, of H^+-birnessite, and K^+-birnessite are shown in Figure 3. The series of *00l* reflections between 10° and 30° in 2θ of the birnessite

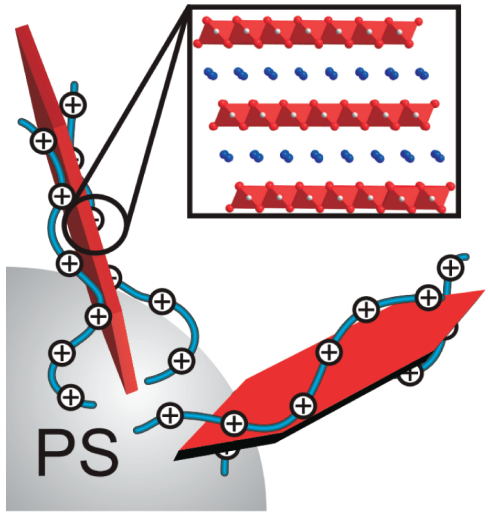

Figure 4. Schematic representation of the stabilization of the layered birnessite structure by the cationic pTMAEMC chains of the SPB. Ultrathin, turbostratically disordered stacks and delaminated lamellae are sandwiched between pTMAEMC chains and thus tightly immobilized by electrostatic forces between SPB carrier and MnO_2NP. The inset shows the crystal structure of a K^+-birnessite (water molecules in the interlayer are not shown).

modifications contain crucial information on the *d*-spacing between consecutive lamellae and the thickness of the stacks and shall therefore be discussed in more detail: The PXRD-analysis shows a regular 3D ordering in the case of the K^+-birnessite. For this material, both the stacking vector and the mutual position of stacked lamellae are well-defined (c^*-ordered). The H^+-birnessite is, however, much less ordered as indicated by, first, a broadening of the *00l* reflections and, second, the absence of any reflections of mixed indices, for instance the *104* reflection which is missing in H^+-birnessite but is clearly visible in case of the K^+-birnessite. Instead of symmetrically shaped peaks of reflections of mixed indices, for H^+-birnessite, besides the *00l* series, only *l*-shaped *hk*-bands are observed in the diffractogram, for instance the *10*-band at 36° in 2θ. This lack of reflections of mixed indices indicates that in H^+-birnessite the individual lamellae are stacked turbostratically meaning that the relative position and/or orientation of adjacent lamellae in the stack are random (c^*-disordered). The *hk*-bands are thus the result of a 2D interference within the plane of the lamellae. Furthermore, the broadening of the *00l* reflections indicates that the stacks formed in H^+-birnessite or considerably thinner than in K^+-birnessite.

The PXRD pattern of the MnO_2NP formed in the composite material are yet again distinctly different as compared to both K^+-birnessite and H^+-birnessite. Please note that the two very broad peaks in the diffractogram of the composite particles at 9.4° and 19.1° (2θ) can be assigned to the bare SPB. In this angular region, neither K^+-birnessite nor H^+-birnessite exhibit any peaks. Besides these peaks due to the SPB carrier, only *hk*-bands are observed. The positions of these are in good agreement with what is found for H^+-birnessite suggesting that the lateral dimensions of the lamellae are similar in H^+-birnessite and the MnO_2NP in the composite

(49) Lu, Y; Spyra, P.; Mei, Y; Pich, A.; Ballauff, M. *Macromol. Chem. Phys.* **2007**, *208*, 254–261.

material. However, most surprisingly, the *00l* series is not visible at all in case of the composite particles. Since the much less intense *10*-band is clearly observable, the basal peaks should also be above the detection limit, and the lack of the *00l*-peaks is therefore not because of the high background caused by the carrier particles. The intensities of the *00l*-peaks can be diminished by three different mechanisms. (1) Random interstratification, meaning that interlayer distances between the individual consecutive lamellae in the stack vary and thus partially destroy the regular alteration of the electron density along the stacking direction. (2) Although utmost precautions have been taken in the sample preparation to minimize texture, a certain degree of preferred orientation in the samples of K^+-birnessite and H^+-birnessite will be unavoidable because of the platty particle morphology, while in the composite material a random orientation of the MnO_2NP is assured by the SPB carrier. This definitive lack of preferred orientation might in turn reduce the intensities of the *00l*-series. While small contributions of random interstratification and reduction of preferred orientation may not be ruled out, the cryoTEM micrographs showing very thin MnO_2NP suggest that the nonvisibility of the basal reflection actually is related to (3) the thickness of the stacks. As the stacks of lamellae become thinner and thinner the fwhm (full width at half-maximum) values will steadily increase and the basal peaks will be broadened and pushed into the background. Finally, the *00l*-series will fade away completely when the material is delaminated into single lamellae. At this stage all inner surfaces (interlamellar space) will have been converted into external surfaces. Thus the lack of *00l* peaks in the diffractogram of the composite material suggests that the MnO_2NP in the composite material will be at least highly exfoliated, possibly even partially delaminated into single lamella. Evidently, single lamellae of birnessite exhibit a strong negative charge that must be balanced by counterions. Here EDX-measurements that will be discussed in the following provide valuable information.

Energy Dispersive X-ray Spectroscopy. The EDX spectrum of the composite particles shows high contents of potassium (K) and chlorine (Cl) (see the Supporting Information, Figure S3). The potassium ions (K^+ ions) refer to either interlayer cations in exfoliated MnO_2NP with birnessite structure or to K^+ ions absorbed to external surfaces of delaminated lamellae. Since the samples have been thoroughly purified by ultrafiltration, the appreciable amount of K^+ ions cannot be explained by the presence of the ions in the aqueous phase. Moreover, because of the positive charge of pTMAEMC chains, other positive ions will be mostly excluded from the brush layer. Hence, we concluded that the K^+ ions are bound to internal or external surfaces of the lamellae of birnessite. Charges at the external surface of the nanoparticles are thus balanced by the pTMAEMC chains and by condensed K^+ ions. The presence of chloride ions (Cl^- ions) indicates that these ions are not completely replaced by the MnO_4^- ions as counterions of the pTMAEMC chains

Table 1. Characterization of the Composite Particles of Cationic SPB and MnO_2NP Used in This Study

sample name	n(TMAEMC): n($KMnO_4$)[a]	rate of $KMnO_4$ addition/ ml/h	m(MnO_2) wt %[b]	T /°C
SPB-MnO_2-1	2/1	40	3.15	RT
SPB-MnO_2-2	2/1	3600	3.08	RT
SPB-MnO_2-5	1/1	40	4.90	RT
SPB-MnO_2-8	2/3	40	6.46	RT
SPB-MnO_2-9	1/1	40	5.79	90

[a] Molar ration of quaternized ammonium groups in the brush layer to the added molar amount of $KMnO_4$. [b] Relating to the solid composite particle.

even if an excess of $KMnO_4$ is used. This indicates that the reduction and condensation reaction of MnO_4^- to form birnessite-type nanoneedles is significantly faster than the exchange of Cl^- and MnO_4^- ions itself.

This is in good agreement with the fact that the dosage rate of $KMnO_4$ solution to the SPB dispersion did not affect the reaction. Furthermore Cl^- ions can only stay inside the brush layer as counterions of pTMAEMC chains. This leads to the conclusion that only a small fraction of the negative charges of the birnessite-type nanoneedles is balanced by the pTMAEMC itself and that the charges are mostly compensated by the K^+ ions in the interlayer which is in good agreement with the K fraction seen in the EDX spectrum. As a consequence, after the reduction of the MnO_4^-, the Cl^- ions have to balance most of the charges of the pTMAEMC chains again. This finding may be used to further increase the total amount of MnO_2NP since the exchange and reduction of MnO_4^- ions should repeatedly be possible. This is in full accord with the above finding that the molar fraction of TMAEMC functional groups can be exceeded by the added $KMnO_4$ leading to an increase in the total MnO_2NP content of the composite particles (table 1).

Combining the results of TEM, PXRD, and EDX, the schematic structure of the composite particles shown in Figure 4 may be derived. Birnessite-type single lamellae and ultrathin, turbostratically disordered stacks of only very few lamellae are sandwiched between cationic pTMAEMC chains and thus are tightly immobilized by electrostatic interactions between the SPB carrier and the negative surface charge of MnO_2NP. Nevertheless, the high contents of K^+ ions found by EDX analysis prove that most of the negative charges of the internal and external surfaces of the birnessite-type nanoparticles are not balanced by pTMAEMC chains bound to the external surface but instead by intercalated and surface-adsorbed K^+ ions, respectively. A penetration/intercalation of the pTMAEMC chains between birnessite lamellae seems not to occur, since the steric hindrance of large ions leads to a decreasing probability for intercalation with increasing ion radius.[28] Instead the pTMAEMC chains interact with the external surface charge only. This is in good agreement with the finding that the length of the nanoparticles does not exceed the size of the polyelectrolyte chains.

Conclusions

A facile route has been developed for the preparation of ultrathin birnessite-type nanoneedles within SPB by in situ reduction of $KMnO_4$ precursor molecules. We conclude that the $KMnO_4$ reacts with the quaternized ammonium groups of the brush polymer to form a p(TMAEM MnO_4) precursor which is directly reduced by the basic environment within the brush layer. This leads to a polyelectrolyte-directed growth and stabilization of the nanoparticles which causes a size limitation of the MnO_2NP by the brush extension. TEM micrographs reveal a collapsed structure of the birnessite nanoparticles immobilized on SPB because of drying effects and the loss of interfacial bound water between the single lamellae. In contrast to this, cryoTEM images confirm the needle-like nanoparticles with an average length of 20 nm and a breadth of 1.6 nm are well distributed among the carrier particle. No MnO_2NP are found in free solution. CryoTEM and the PXRD analysis point out that the needles exhibit a c^*-disordered birnessite type structure of the MnO_2. The excess charge of these nanoneedles is mostly balanced by K^+ ions which could be inferred from the EDX analysis. Hence, we obtained ultrathin birnessite-type nanostructures without further delamination processes. Moreover, the composites of the SPB and the nanoparticles exhibit an excellent colloidal stability. These properties make the composite particles a promising material for applications in catalysis. Work along this direction is under way.

Acknowledgment. We thank the Deutsche Forschungsgemeinschaft, Sonderforschungsbereich 840 Bayreuth and the Henkel AG & Co. KGaA for the financial support. The authors are indebted to Benjamin Gossler for EDX measurements.

Supporting Information Available: Additional information contained in Figures S1−S3. This material is available free of charge via the Internet at http://pubs.acs.org.